

## Earth's Alfvén wings driven by the April 2023 Coronal Mass Ejection

Li-Jen Chen<sup>1</sup>, Daniel Gershman<sup>1</sup>, Brandon Burkholder<sup>1</sup>, Yuxi Chen<sup>2</sup>, Menelaos Sarantos<sup>1</sup>, Lan Jian<sup>1</sup>, James Drake<sup>3</sup>, Chuanfei Dong<sup>2</sup>, Harsha Gurram<sup>1,3</sup>, Jason Shuster<sup>4</sup>, Daniel B. Graham<sup>5</sup>, Olivier Le Contel<sup>6</sup>, Steven J. Schwartz<sup>7,8</sup>, Stephen Fuselier<sup>9</sup>, Hadi Madanian<sup>8</sup>, Craig Pollock<sup>10</sup>, Haoming Liang<sup>1,3</sup>, Matthew Argall<sup>4</sup>, Richard E. Denton<sup>11</sup>, Rachel Rice<sup>1,3</sup>, Jason Beedle<sup>4</sup>, Kevin Genestreti<sup>4,9</sup>, Akhtar Ardakani<sup>4</sup>, Adam Stanier<sup>12</sup>, Ari Le<sup>12</sup>, Jonathan Ng<sup>1,3</sup>, Naoki Bessho<sup>1,3</sup>, Megha Pandya<sup>1</sup>, Frederick Wilder<sup>13</sup>, Christine Gabriele<sup>14</sup>, Ian Cohen<sup>15</sup>, Hanying Wei<sup>16</sup>, Christopher T. Russell<sup>16</sup>, Robert Ergun<sup>8</sup>, Roy Torbert<sup>4,9</sup>, James Burch<sup>9</sup>

1 NASA Goddard Space Flight Center, Greenbelt, MD, USA

2 Boston University, Boston, MA, USA

3 University of Maryland, College Park, MD, USA

4 University of New Hampshire, Durham, NH, USA

5 Swedish Institute of Space Physics, Uppsala, Sweden

6 CNRS/Ecole Polytechnique/Sorbonne Université/Univ. Paris Sud/Observatoire de Paris, Paris, France

7 Imperial College London, London, UK

8 Laboratory for Atmospheric and Space Physics, University of Colorado Boulder, Boulder, CO, USA

9 Southwest Research Institute, San Antonio, TX, USA

10 Denali Scientific, Healy, Alaska, USA

11 Dartmouth College, Hanover, NH

12 Los Alamos National Laboratory, Los Alamos, NM, USA

13 University of Texas at Arlington, Arlington, TX, USA

14 The Aerospace Corporation, El Segundo, CA, USA

15 The Johns Hopkins University Applied Physics Laboratory, Laurel, MD, USA

16 University of California, Los Angeles, Los Angeles, CA, USA

### Plain Language Summary

Like supersonically fast fighter jets creating sonic shocks in the air, planet Earth typically moves in the magnetized solar wind in super-Alfvénic speeds and generates a bow shock. Here we report unprecedented observations of Earth's magnetosphere interacting with a sub-Alfvénic solar wind brought by an erupted magnetic flux rope from the Sun in the form of a coronal mass ejection (CME). The terrestrial bow shock disappears, leaving the magnetosphere exposed directly to the cold CME plasma and the strong magnetic field from the Sun's corona. Our results show that the magnetosphere transforms from its typical windsock-like configuration to having wings that magnetically connect our planet to the Sun. The wings are highways for Earth's plasma to be lost to the Sun, and for the plasma from the foot points of the Sun's erupted flux rope to access Earth's ionosphere. Our work presents new opportunities to study interaction between astrophysical bodies with sub-Alfvénic plasma wind in our solar and other stellar systems.

### Abstract

We report Magnetospheric Multiscale observations of the dayside magnetosphere when the solar wind becomes sub-Alfvénic, causing the windsock-like magnetosphere to transform into Alfvén

wings. The event occurred in the magnetic cloud of a Coronal Mass Ejection (CME) on April 24, 2023. We highlight the following outstanding features: (1) a layer of accelerated cold CME flow directly adjacent to the wing and to the magnetopause, presenting a rare regime of magnetosphere interaction with unshocked CME plasma; (2) wing filaments created by magnetic reconnection, representing new channels of magnetic connection between the magnetosphere and foot points of the Sun's erupted flux rope; (3) cold CME ion deceleration with little heating across the magnetopause. The reported measurements advance our knowledge of CME interaction with planetary magnetospheres, and open new opportunities to understand how sub-Alfvénic plasma flows impact astrophysical bodies such as Mercury, moons of Jupiter, and exoplanets close to their host stars.

## **Introduction**

An erupted magnetic flux rope from the Sun in the form of fast Coronal Mass Ejection (CME) arrives at the Earth on April 24, 2023. Within the flux rope is a lower density plasma parcel that brings the local Alfvén speed to above the solar wind speed for two hours, providing the magnetosphere a sub-Alfvénic solar wind condition. MHD simulations [Ridley, 2007; Chané et al., 2015; Chen et al., 2024] have shown that during long duration ( $> 1$  hour) sub-Alfvénic solar wind, Earth's magnetosphere transforms into Alfvén wings, a configuration analogous to Jupiter's moons as they reside in the sub-Alfvénic flow of the Jovian magnetosphere [Kivelson et al., 2004; Wang et al., 2018; Zhou et al., 2019].

To date, observations of Earth's magnetosphere interaction with long-duration sub-Alfvénic solar wind have only been reported in three prior papers. Magnetic field and ion flow measurements by Geotail at GSE [ $X \sim (-11: -20)$ ,  $Y \sim (28: 23)$ ,  $Z \sim 5$ ]  $R_E$  captured the dusk Alfvén wing and an enhanced flow layer immediately outside of the reduced flow region of the wing [Chané et al., 2012]. The plasma properties (e.g., density, temperature, and energy distribution) of the enhanced flow layer were not measured. The observations by Lugaz et al. [2016] focus primarily on radiation-belt electron loss, and observed neither the enhanced flow layer nor the Alfvén wings. The work by Hajra and Tsurutani [2022] shows statistics of the sub-Alfvénic solar wind properties and associated changes in the geomagnetic fields in the inner magnetosphere as well the ionosphere, and does not address the Alfvén wings. In this paper, we report dayside measurements from the Magnetospheric Multiscale (MMS) mission [Burch et al., 2016]. This event is the only time a long duration sub-Alfvénic solar wind occurs in the mission life of MMS so far. With its unprecedented high-cadence three-dimensional plasma measurements, MMS records a rare regime of magnetopause reconnection in which channels of magnetic connection between the Sun's erupted flux rope and Earth's magnetic fields are created.

## **Observations**

For sub-Alfvénic solar wind with a dominant dawn-dusk ( $y$ ) IMF, global MHD simulations [Chané et al., 2015; Chen et al., 2024] demonstrate the formation of dawn-dusk wings. In the April 2023 CME at  $\sim 14$  UT, MMS approaches the southern dawn wing on the dayside at GSE [ $10.7, -7.9, -6.8$ ]  $R_E$ . The presented magnetic fields are measured by the Flux Gate Magnetometer [Russell et al., 2016], thermal plasma Fast Plasma Investigation [Pollock et al., 2016], and nonthermal particles Fly's Eye Energetic Particles spectrometers [Blake et al., 2016] onboard MMS2. Vectors are shown in the Geocentric Solar Ecliptic (GSE) coordinate system.

We begin with an overview of the CME in relation to the geomagnetic storm development (Figure 1). The fast-moving CME created an interplanetary (IP) shock and a sheath region in front of the expanding flux rope (Figure 1a), the magnetic cloud (MC). Arrival of the IP shock and the southward IMF in the CME sheath initiate the main phase of a geomagnetic storm. The storm development stalls as the IMF  $B_z$  turns from southward to northward in the CME sheath and stays mostly northward until entry into the MC where  $B_z$  is strongly southward (Figures 1b and 1g). In the MC, IMF  $B_z$  slowly rotates from strongly southward to northward. The CME sheath (bounded by the cyan and magenta vertical lines) is prominently marked by (1) enhanced fluxes of 60-560 keV electrons and ions with the strongest fluxes and highest energy reached at the IP shock arrival (Figures 1c-1d), and (2) the IMF southward turning (Figure 1b) and density drop (Figure 1e). The accelerated particles at the IP shock attain energies even higher than those in the shown inner-magnetosphere interval ( $\sim 17$  UT on 2023-04-24). In the MC, MMS encountered Earth's bow shock five times (marked as red arrows in Figure 1b). MMS registers a double-peak density pulse at the second bow shock crossing (Figure 1e), coincident with a spike in  $M_A$  (Figure 1f) and a bipolar pulse in SYM-H (Figure 1g). This bow shock crossing has been analyzed in depth [Graham et al., 2023]. The density pulse consists of three ion species (a subject of forthcoming papers), and results in extreme responses of the geomagnetic field [Despirak et al., 2023].

MMS monitors the magnetosheath interaction with the MC continuously after its last bow shock crossing at  $\sim 4:20$  UT (Figures 1b, 1e), and particularly as the solar wind Alfvén Mach number  $M_A = V_{sw}/V_A$  (where  $V_{sw}$  is the solar wind speed and  $V_A$  is the Alfvén speed) drops and rises back and forth culminating in the two-hour interval ( $\sim 12:30$ - $14:30$  UT) when  $M_A$  stays at  $\sim 0.6$  (Figure 1f). The sub-Alfvénic solar wind is caused by the low density and high IMF strength in the MC rather than a decrease in  $V_{sw}$  (Figures 1e and 1h). The interval is concurrent with a SYM-H plateau at  $\sim -120$  nT (Figure 1g), indicating that the ring current intensity is being held at a level stronger than that of most geomagnetic storms. We show the Wind magnetic field measurements (Figure 1a; without any time shift to preserve its original variations) to enable discernment of magnetic variations from the CME magnetic cloud and those due to interaction with Earth's magnetosphere. At approximately  $14:30$  UT, MMS observes the closed-field-line region of the magnetosphere with the magnetic field components similar to those observed in the magnetosphere ( $\sim 17$  UT).

MMS observes the Earth's magnetosheath plasma evolving from shocked (decelerated and heated; marked by the first magenta bar in Figure 2) to unshocked solar wind (beginning is marked with a blue arrow) just before 13 UT, and back to the shocked solar wind after  $\sim 1440$  UT (second magenta bar). During the interval when  $M_A < 1$ , the bow shock becomes weaker, farther away, and eventually disappears [Ridley et al. 2007]. Characteristics of the unshocked solar wind include well-defined narrow energy bands of the cold proton and alpha particles (Figure 2c) at energies consistent with upstream measurements such as those from THEMIS B (Figure 2h). The unshocked solar wind flow registered by MMS shows an increase (Figure 2b) consistent with MHD simulation results [Chen et al., 2024]. MMS measures the plasma in the layer of enhanced flow to be cold and unthermalized low-beta wind within the CME flux rope. Note that this layer of cold and accelerated CME plasma is now the immediate upstream of the wings and magnetopause.

In contrast to the enhanced flows at the MMS location, THEMIS B in the solar wind on the dayside (at GSE [34.6, 48.5, 4.5]  $R_E$  at 14 UT) orbiting the Moon does not observe the increasing flow, rather,  $V \sim V_{ix} \sim -500$  km/s from 13:30 to 16 UT (Figure 2g). The solar wind flow from OMNI is  $\sim 550$  km/s (Figure 1h; observed at L1 and propagated to the model bow shock nose) not showing the increase observed by MMS (Figure 2b), either. The correlated discontinuities in THEMIS B magnetic field (Figure 2f) and ion energy distribution (2h) correspond to the bow shock crossings the spacecraft (right before and after 10UT, just after 11 UT, and after 16 UT), indicating that the bow shock expands to the Moon distance as  $M_A$  approaches 1 from above.

At  $\sim 14:30$  UT when  $V_i \sim 0$ , the density and magnetic field components resemble those in the magnetosphere ( $\sim 16:30$  UT in Figure 2). The strongly positive  $B_z$  and  $B_x$  ( $> \sim 20$  nT) are consistent with MMS entry of the magnetosphere from the southern hemisphere just outside (equatorward) of the cusp (if entry into the magnetosphere is inside the cusp,  $B_z$  would be negative). The weak negative  $B_y$  is consistent with the pre-noon location of MMS. However, the energy distributions of ions and electrons (negligible ion flux below 100 eV; weaker ion flux above  $\sim 3$  keV; electron flux enhancement only below 5 keV) are distinct from those in the magnetosphere at  $\sim 16:30$  UT. The plasma properties suggest that this closed field line region is a freshly formed during the storm, and possibly during the sub-Alfvénic interval.

In the zoom-in interval (Figures 2i-2o), MMS begins to encounter magnetic flux tubes with distinctly more energetic plasmas than the unshocked CME MC plasma (Figures 2k, 2m). Ions with energies 20 keV and above are observed, while the MC protons are at  $\sim 3$  keV and alpha particles at  $\sim 6$  keV (Figure 2k). The flux of energized electrons peaks at 200-1000 eV, in contrast to the MC electron flux maximizing below 200 eV at  $\sim 14:07$  UT (Figure 2m). Isolated flux tubes (sandwiched by MC intervals) correspond to excursions in the magnetic field (Figure 2i) and ion velocity (Figure 2j), energized or thermalized MC ions (Figure 2k), and density spikes (Figure 2l). We name these isolated flux tubes (14:05-14:24 and 14:37-14:38 UT) filaments. The filaments contain field lines with at least one end connected to the Earth, an interpretation based on the assumption that the energized electrons and ions are either of Earth origin or due to interaction between the MC and the magnetosphere such as reconnection. This assumption is supported by the fact that the  $V_{iy}$  velocities tend to be stronger than the ambient MC flow along  $-y$ , indicating strong downward motion that is consistent with reconnected flux tubes moving toward dawn, and not consistent with motion in and out of the magnetosphere. Prior to the shown interval, MMS registers the MC plasma and field lines which have both ends at the Sun.

Upon exit from the magnetosphere and back into the enhanced MC flow layer, MMS detects the MC proton energy at 3-4 keV, corresponding to velocities 750-850 km/s, and then drops to 1-2 keV (Figure 2k). The ion energy drop occurs with a sudden density increase (Figure 2l), signaling the end of the sub-Alfvénic interval locally at MMS. After the density rise, ions regain their “shocked” appearance. A corresponding density rise is observed by Wind and THEMIS B spacecraft (not shown) at L1 and the Moon, respectively.

From 14:25 to 14:35 UT, MMS probes a primarily closed field line region. Enhanced fluxes of 60-150 keV electrons (Figure 2n) at pitch angles approximately 90 degrees (Figure 2o) are

interpreted as the closed field line regions based on the following: (1) the pitch angle distribution peaks at approximately 90 degrees, consistent with electrons being trapped. (2) Examination of parallel and perpendicular temperatures of lower energy (0.01-20keV) electrons rules out that the energetic electron flux peaking at 90 degrees is due to perpendicular heating (data not shown; full characterization of the electron distribution functions is forthcoming in a separate study). (3) Ion flows are stagnant or weak, and ions and electrons are hot, consistent with the expected magnetosphere condition. (4) The magnetic field is roughly consistent with expected Earth's magnetic field with  $B_z > 0$ ,  $B_x > 0$ , and  $B_y < 0$  at the MMS location. (5) The density ( $0.25 \text{ cm}^{-3}$ ) is consistent with magnetospheric density, and lower than the MC density ( $0.5 \text{ cm}^{-3}$ ).

We zoom in the entry (first green bar in Figure 2l) and exit (second green bar) intervals to highlight the filaments and ion mixing/deceleration/heating (Figure 3). We interpret regions with no discernable field-aligned anisotropy as having closed field lines (such as that at 14:40 UT in Figures 3b1-c1), and hence part of the magnetosphere. Intervals with stronger parallel (to  $\mathbf{B}$ ) flux of electrons above 1 keV than anti-parallel (marked by cyan bars and shaded) are interpreted as dawn-wing filaments generated by reconnection in the southern hemisphere. These intervals tend to have hot ions, and less discernable cold MC ions. The parallel electrons above 1 keV are interpreted as energized by southern cusp reconnection (depicted by the southern-cusp red arrow in Figure 4h). The ions in the interval 14:23:20-14:23:23UT maintain their MC-like cold temperature, and both parallel and anti-parallel electrons below 200 eV exhibit MC-like energy distribution in addition to the keV parallel electrons, showing mixing of MC plasma with reconnection-energized plasma. Note that based on examination of the global MHD simulations [Chen et al., 2024], the most probable southern cusp reconnection locations are primarily on the duskside of the Earth, and of order  $10 R_E$  away from MMS. For reference, electrons at 1 keV travel this distance in 1.8 s.

Anti-parallel electron flux (Figure 3c2) at  $\sim 1$  keV are observed to dominate over the parallel flux (Figure 3b2) in the magenta intervals with cold MC-like ions (Figure 3a2), providing evidence for CME IMF field lines that have just been newly reconnected at locations north of MMS. Note that the parallel flux exhibits an energy distribution similar to the ambient MC electron energy distribution (such as that at  $\sim 14:38:15$ UT). The corresponding ion reduced distributions in  $v_{ixyz}$  (Figures 3d2-f2) further show that the ions are approximately the cold MC ions.

The ion  $v_{ixyz}$  distributions reveal ion deceleration, thermalization, and mixing under the unusual condition of the cold unshocked solar wind directly coming against the magnetopause and the Alfvén wing. Cold MC ions penetrate into the closed field line region, such as those in the intervals centered at  $\sim 14:23:26$ ,  $14:23:40$ ,  $14:23:55$  UT (Figures 3d1-f1), and at  $14:36:05$  UT (Figures 3d2-f2). Some of the cold MC ions are decelerated to  $v_{ix} \sim 0$  ( $\sim 14:23:40$  UT), and their distribution in  $v_{iy}$  is altered from peaking at  $-300$  km/s to  $100$  km/s, while keeping  $v_{iz}$  approximately the same as the ambient MC  $v_{iz} \sim -300$  km/s. Ions observed in the interval between  $14:36:15$ - $14:36:27$  UT are hot with no discernable cold solar wind-like populations, and the distribution is relatively symmetric with respect to  $v_{ix} = 0$ , while biased toward positive  $v_{iz}$  and negative  $v_{iy}$ , indicating a northward and dawnward flow on closed field lines (field line topology inferred from the roughly equal parallel and anti-parallel electron flux). Apart from this interval, MMS observes clear trace of the cold solar wind ion population as it exits back to the unshocked solar wind, even when the population has been decelerated.

We zoom in example filaments in the interval 14:08:00 to 14:09:20 UT (red bar in Figure 2l) to show structures and dynamics of the plasma (Figure 4). The cold proton population is at  $\sim 2$  keV. The filaments exhibit magnetic field (Figure 4a) and ion flow (Figure 4g) excursions, energized ions (Figure 4b), flux enhancements of energized keV electrons parallel (Figure 4c) and anti-parallel (Figure 4d) to  $\mathbf{B}$ , electron density spikes and depressions (Figure 4e) within. The ion phase space distribution in  $v_{ix}$  indicate that the filaments before 14:08:20 UT are substantially colder than those afterward (Figure 4f), interpreted as due to different ‘age’ with the filaments with colder and more energetic ions being younger (newly reconnected). If reconnection occurs farther away from MMS, lower energy ions can have access to the spacecraft.

As illustrated in Figure 4h based on data from a global MHD simulation [Chen et al., 2024], two types of field lines are the most likely at the MMS location: (a) closed field lines (green), and (b) dawn wing (red) - southern hemisphere field lines connected to the CME flux rope - produced by reconnection occurring in the southern hemisphere yielding energized electrons parallel to  $\mathbf{B}$  at the MMS location (Figure 4h “newly reconnected” red field line and the red arrow on green field line are simulation examples; blue shaded intervals in Figures 3b1-c1 are MMS examples), and the northern hemisphere, giving rise to energized electrons anti-parallel to  $\mathbf{B}$  (red arrow as one example reconnection site for the “to be reconnected” green field line in Figure 4h; magenta shaded intervals in Figures 3b2-c2). These field lines are traced from the surface of  $r = 3 R_E$  from uniformly distributed seed points covering the entire 3D sphere, representative of all possible field line topologies within the simulation. The open field lines extending towards dawn (red) and dusk (blue) form two wings connecting the Earth and the Sun magnetically.

The stormtime field line connectivity resulted from active reconfiguration of the 3D magnetosphere may allow MMS to observe dusk wing field lines. Specifically, field lines coming out of the southern-dusk sector may go into the northern hemisphere on the dawn side, such that upon reconnection in the southern-dusk hemisphere, the dayward and duskward convection of the field line will bring it across MMS. The implication is that dusk wing and dawn wing open field lines may either meet on the dayside and produce closed field lines, or reconnect with draped IMF field lines, giving rise to dual reconnection (analogous to but distinct from the dual-lobe reconnection under northward IMF and super-Alfvénic solar wind [Fuselier et al., 2014]). On the other hand, if few closed field lines cross from southern-dusk to northern-dawn, MMS is unlikely to observe the dusk wing field lines, because reconnection occurring duskward of MMS in the southern hemisphere and northward of MMS in the northern hemisphere (blue “newly reconnected” field line in the southern hemisphere and the three white field lines in the northern hemisphere are examples) produce new dusk-wing field lines which convect duskward and unlikely cross the path of MMS in the dayside southern dawn sector.

## Summary and Discussion

During the April 2023 CME when the solar wind is sub-Alfvénic, MMS monitors the magnetosheath evolving from shocked to unshocked solar wind, and observes outstanding features: (1) in the CME MC, a layer of accelerated cold solar wind flow adjacent to the dawn wing and the magnetopause, (2) filaments of the Alfvén wing moving faster than the ambient MC flow and representing new channels of magnetic connection between Earth’s magnetosphere and the foot points of the Sun’s erupted flux rope, and (3) cold CME MC ions penetrating into

the closed field line region with substantial deceleration yet little heating. In other words, just inside the magnetopause is where the MC solar wind plasma gets decelerated, in contrast to the typical super-Alfvénic solar wind condition under which the first major deceleration and heating of the solar plasma occurs at the bow shock several  $R_E$  upstream from the magnetopause.

The sub-Alfvénic solar wind interaction with the magnetosphere creates a rare regime of magnetopause reconnection. Instead of the usual magnetosheath with heated and decelerated solar wind, now the immediate magnetopause upstream is cold and accelerated CME plasma on MC field lines. The beta in this CME flux rope is as low as 0.01, in contrast to the typical magnetosheath  $\beta > 1$ . Lower beta has been demonstrated to support faster reconnection [Zenitani and Miyoshi, 2020], and stronger production of nonthermal particles [Li et al., 2021]. The magnetopause reconnection with the low beta CME solar wind as its upstream resembles that at the inner planets (such as Mercury [e.g., Sarantos and Slavin, 2009]) of the solar system and at magnetized exoplanets close to their stars.

What prevents the ring current from being dissipated during the sub-Alfvénic interval? SYM-H stays approximately constant at -120 nT, prolonging the storm recovery. Do injections of energetic ions occur to replenish the ring current at a rate roughly balancing the loss? If so, how do the injections relate to nightside magnetic reconnection under the Alfvén-wing magnetosphere configuration?

Sun-Earth magnetic connection through Alfvén wings is analogous to the Jupiter-Ganymede connection. Accelerated field-aligned electrons at the magnetopause as well as auroral emissions at Ganymede support magnetic reconnection occurrence [Ebert et al, 2022; Gershman et al., 2024]. Here at Earth, MMS measurements of the Alfvén wing filaments indicate that newly reconnected flux bundles become part of the wings, continuously replenishing the wings. MMS observations of this MC-magnetosphere interaction indicate that the Earth loses its plasma to the solar corona through the wings, and suggest that Ganymede aurora is likely powered by magnetic reconnection. Conversely, electrons from the foot points of the Sun's erupted flux rope may be accelerated and precipitate into Earth's ionosphere to form Alfvén wing aurora – a possibility to be checked out by future work.

### **Open Research**

MMS data are publicly available at <https://lasp.colorado.edu/mms/sdc/public/about/browse-wrapper/>. Wind and THEMIS B data are obtained from the CDAWeb <https://cdaweb.gsfc.nasa.gov/index.html/>.

### **Acknowledgments**

This work is supported by the NASA MMS Mission.

### **References**

Burch, J. L., Torbert, R. B., Phan, T. D., Chen, L. J., Moore, T. E., Ergun, R. E., et al. (2016). Electron-scale measurements of magnetic reconnection in space. *Science*, 12, aaf2939. <https://doi.org/10.1126/science.aaf2939>

Blake, J. B., Barry Mauk, et al. (2016). The Fly's Eye Energetic Particle Spectrometer (FEEPS) Sensors for the Magnetospheric Multiscale (MMS) Mission, *Space Sci Rev* 199, 309–329 (2016). <https://doi.org/10.1007/s11214-015-0163-x>

Chané, E., Saur, J., Neubauer, F., Raeder, J., & Poedts, S. (2012). Observational evidence of Alfvén wings at the Earth. *Journal of Geophysical Research: Space Physics*, 117 (A9).

Chané, E., Raeder, J., Saur, J., Neubauer, F., Maynard, K., & Poedts, S. (2015). Simulations of the earth's magnetosphere embedded in sub-Alfvénic solar wind on 24 and 25 May 2002. *Journal of Geophysical Research: Space Physics*, 120 (10), 8517–8528.

Chen, Yuxi, Chuanfei Dong, Li-Jen Chen, Menelaos Sarantos, Brandon Burkholder (2024), Interplanetary magnetic field By controlled Alfvén wings at Earth during encounter of a coronal mass ejection, arXiv:2402.04282

Fuselier, S. A., S. M. Petrinec, K. J. Trattner, and B. Lavraud (2014), Magnetic field topology for northward IMF reconnection: Ion observations, *J. Geophys. Res. Space Physics*, 119, doi:10.1002/2014JA020351.

Gershman, D.J., et al. (2024), Magnetic reconnection at planetary bodies and astrospheres, *Space Science Reviews*, <https://doi.org/10.1007/s11214-023-01017-2>

Graham, D. B., Yu. V. Khotyaintsev, A. P. Dimmock, A. Lalti, J. J. Boldu, S. F. Tigik, S. A. Fuselier (2023). Ion Dynamics Across a Low Mach Number Bow Shock, arXiv:2311.11373

Li, X., et al. (2017), Particle Acceleration during Magnetic Reconnection in a Low-beta Plasma, *2017 ApJ* 843, 21, DOI: 10.3847/1538-4357/aa745e

Lugaz, N., Farrugia, C. J., Huang, C.-L., Winslow, R. M., Spence, H. E., and Schwadron, N. A. (2016). Earth's magnetosphere and outer radiation belt under sub-Alfvénic solar wind. *Nature Communications*, 7, 13001.

Kivelson, M., Fran Bagenal, William Kurth, Fritz Neubauer, Chris Paranicas, Joachim Saur (2004), Magnetospheric Interactions with Satellites, In: *Jupiter. The planet, satellites and magnetosphere*. Edited by Fran Bagenal, Timothy E. Dowling, William B. McKinnon.

Pollock, C., Moore, T., Jacques, A., Burch, J., Gliese, U., Saito, Y., et al. (2016). Fast Plasma Investigation for Magnetospheric Multiscale. *Space Sci. Rev.*, 199, 331-406. doi: 10.1007/s11214-016-0245-4

Ridley, A. J. (2007). Alfvén wings at earth's magnetosphere under strong interplanetary magnetic fields. *Annales Geophysicae*, 25 (2), 533–542.

Russell, C. T., Anderson, B. J., Baumjohann, W., Bromund, K. R., Dearborn, D., Fischer, et al. (2016). The magnetospheric multiscale magnetometers. *Space Sci. Rev.*, 199 , 189-256. doi: 10.1007/s11214-014-0057-3

Sarantos, M., and J. A. Slavin (2009), On the possible formation of Alfvén wings at Mercury during encounters with coronal mass ejections, *Geophys. Res. Lett.*, 36, L04107, doi:10.1029/2008GL036747.

Wang, L., et al. (2018), Electron Physics in 3-D Two-Fluid 10-Moment Modeling of Ganymede's Magnetosphere, *JGR - Space Physics* (2018) <https://agupubs.onlinelibrary.wiley.com/doi/10.1002/2017JA024761>

Ebert, R. W., et al. (2022), Evidence for Magnetic Reconnection at Ganymede's Upstream Magnetopause During the PJ34 Juno Flyby, *Geophysical Research Letters* (2022). <https://agupubs.onlinelibrary.wiley.com/doi/full/10.1029/2022GL099775>

Zenitani, Seiji, and Takahiro Miyoshi (2020). Plasmoid-dominated Turbulent Reconnection in a Low- $\beta$  Plasma, *The Astrophysical Journal Letters*, 894:L7

Zhou, H., Toth, G., Jia, X., Chen, Y., and Markidis, S. (2019). Embedded kinetic simulation of Ganymede's magnetosphere: Improvements and inferences. *Journal of Geophysical Research: Space Physics*, 124 (7), 5441–5460.

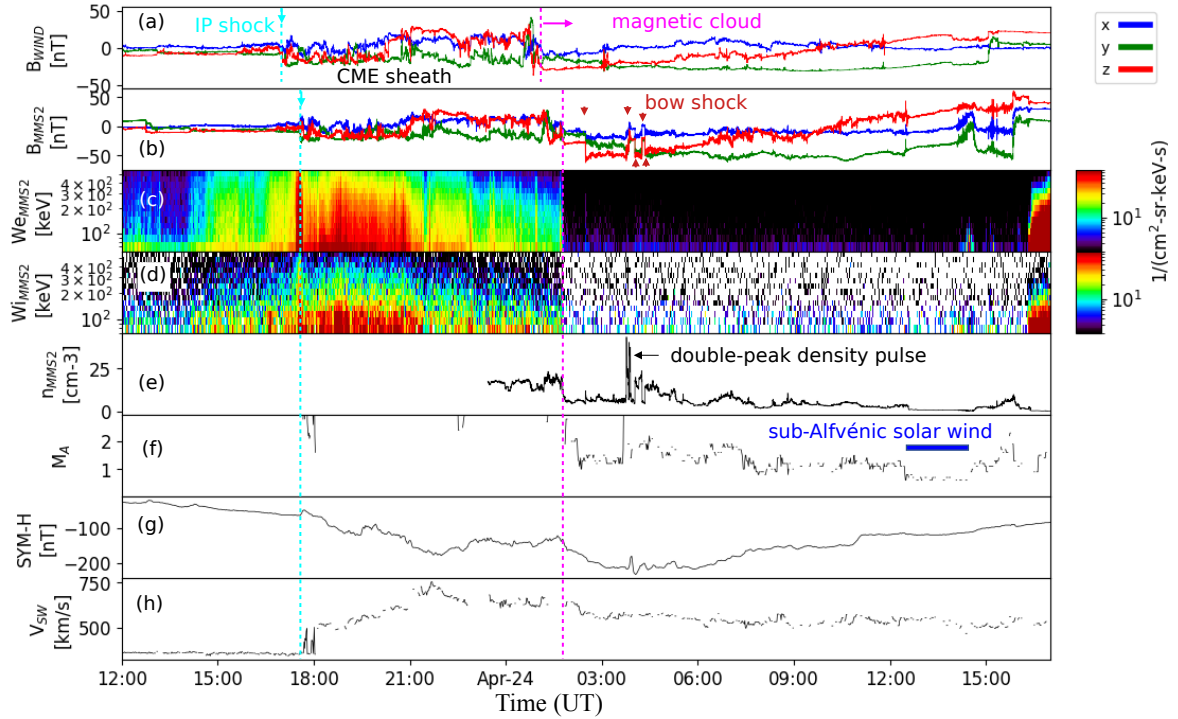


Figure 1. Overview of the 2023 April CME and the associated geomagnetic storm. (a) Three components of the magnetic field observed by the Wind spacecraft at L1, and (b) by MMS2 on the dayside, respectively. (c-d) MMS suprathermal electron and ion (60-550 keV) energy fluxes. (e) MMS electron density. (f) Alfvén Mach number  $M_A$  (from the OMNI data which have been propagated to the model bow shock nose) drops below 2 upon entry into the magnetic cloud (CME flux rope) where the energetic particle flux enhancements cease. The two-hour interval when  $M_A \sim 0.6$  is the primary focus of this paper. (g) Geomagnetic storm index SYM-H. (h) Solar wind speed from OMNI.

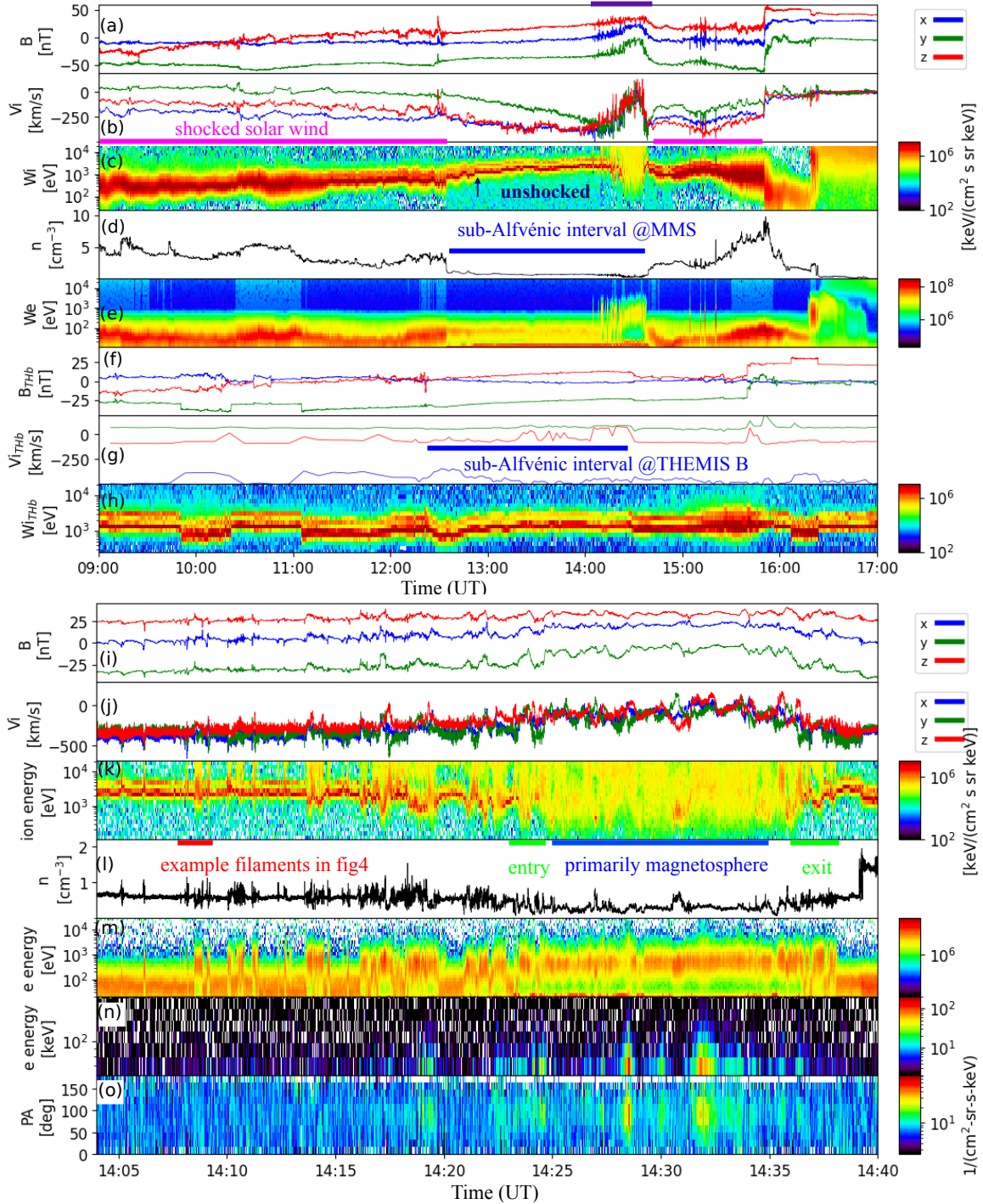


Figure 2. MMS observation of the magnetosheath evolution, Alfvén wing filaments, and stormtime magnetosphere. (a) Magnetic field. (b) Ion velocity. (c) Ion energy flux. (d) Electron density. (e) Electron energy flux. (f-h) Magnetic field, ion velocity, and energy flux from THEMIS B (orbiting the Moon at GSE [34.6, 48.5, 4.5]  $R_E$  at 14 UT) to provide a near-Earth upstream context. The MMS interval 14:04-14:40 UT (purple bar) is zoomed in to highlight the filaments and distinct electron regions, based on (i) magnetic field, (j) ion flow, (k) energy flux of ions (0.2-20 keV), (l) plasma density, (m) energy flux of electrons (0.02-3 keV), and (o-p) energetic electron flux (60-200 keV) and their pitch angle (PA) distribution.

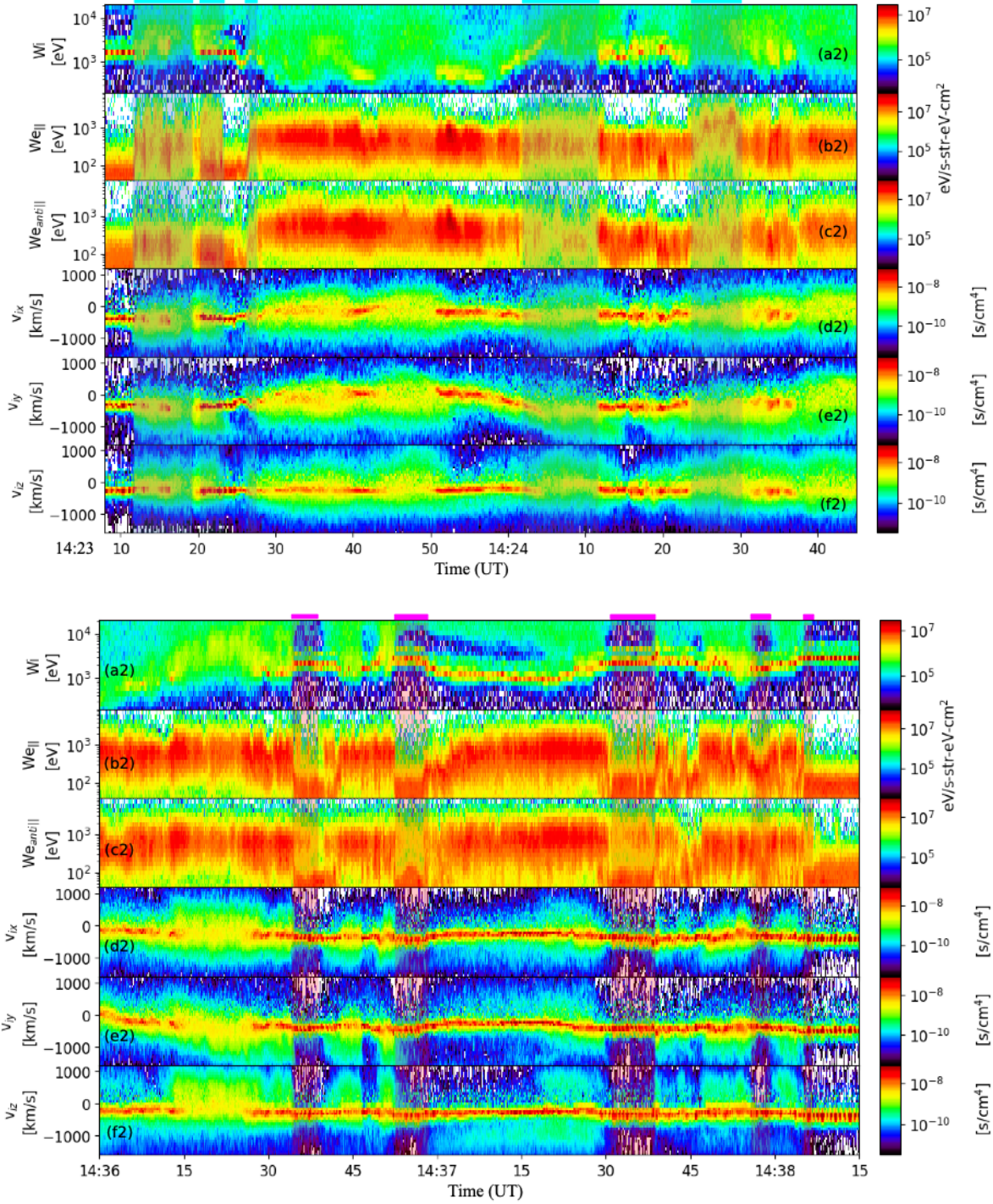


Figure 3. Evidence for the southern/dawn wing flux tubes and cold MC ion deceleration. Entry (a1-f1) into and exit (a2-f2) from the closed field line region of the magnetosphere. (a1,a2) ion energy flux to provide a context for distinct plasma regions based on the cold MC and the hot ions. (b1,b2) electron energy flux parallel to  $\mathbf{B}$ . (c1,c2) electron energy flux anti-parallel to  $\mathbf{B}$ . Ion phase space density (summed over the other two velocity dimensions) as a function of  $v_{ix}$  (d1,d2),  $v_{iy}$  (e1,e2), and  $v_{iz}$  (f1,f2). The cyan (magenta) bars and the shades below them mark the intervals with dominant parallel (anti-parallel) electron fluxes at approximately 1 keV.

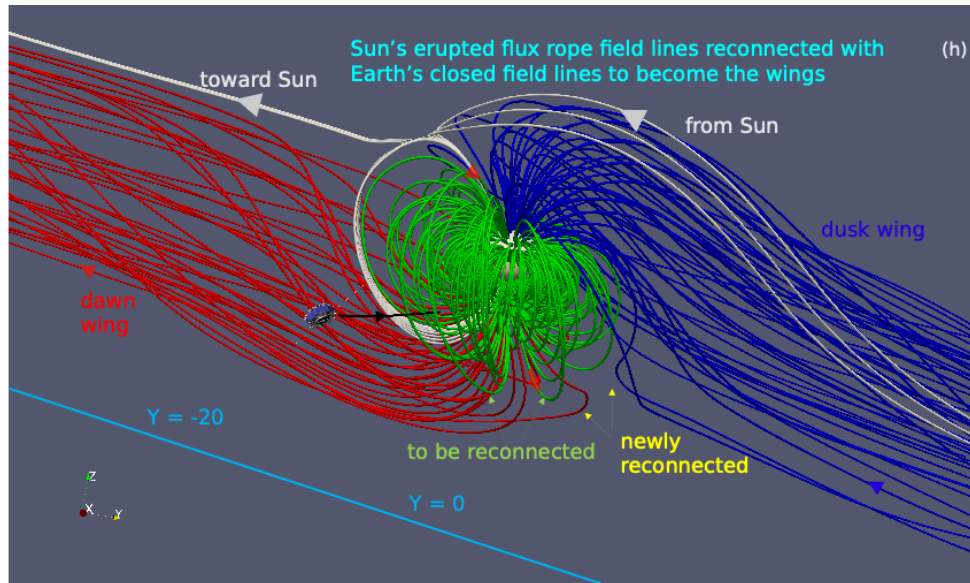
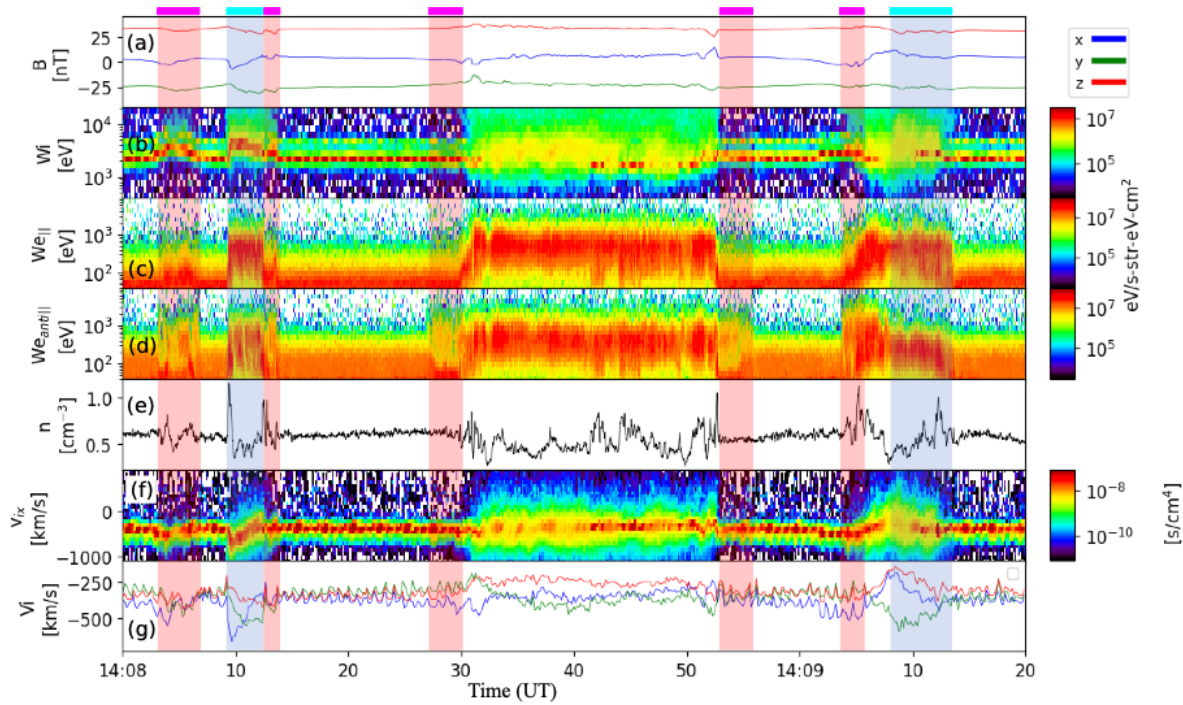


Figure 4. Zoom-in of example filaments and a global field-line illustration. (a) Magnetic field. (b) Energy flux of ions (0.4-20 keV) summed over all directions. (c-d) Energy flux of electrons (0.02-30 keV) parallel and antiparallel to  $B$ . (e) Electron density. (f) Ion phase space density (summed over  $v_y$  and  $v_z$ ) as a function of  $v_x$ . (g) Ion flow vector. (h) Illustration of the CME flux rope field lines interacting with Earth's Alfvén-wing magnetosphere. The southern-dawn wing is in red, northern-dusk wing blue, closed field lines green, and example newly reconnected as well as soon-to-be-reconnected field lines white. Red arrows on green field lines above and below the Earth show example locations for potential reconnection.